Hindawi
Journal of Food Biochemistry
Volume 2023, Article ID 6637700, 16 pages
https://doi.org/10.1155/2023/6637700

Research Article

Ursolic Acid Inhibited Cholesterol Esterase and Pancreatic Lipase Activities and Decreased Micellar Cholesterol Solubility *In Vitro*

Wenjing Jiang,[1] Qun Huang,[2] Xiangxing Meng,[1] Rizwan-ur Rehman,[3] Kun Qian,[1] Xu Yang,[4] Xiaozhi Liu,[5] Jingnan Chen,[6] Ye Zhang,[1] Jing Li,[1] Jilite Wang,[7] Qingbin Guo,[1] Suwen Liu,[8] and Hao Wang[1]

[1]*State Key Laboratory of Food Nutrition and Safety, Tianjin University of Science and Technology (TUST), Tianjin 300457, China*
[2]*The Key Laboratory of Environmental Pollution Monitoring and Disease Control, Ministry of Education, Guizhou Medical University, Guiyang, Guizhou 550025, China*
[3]*Department of Bioinformatics and Biosciences, Capital University of Science and Technology, Zone V, Kahuta Road, Islamabad, Pakistan*
[4]*National Center of Supervision and Inspection for Processed Food Quality, Tianjin Institute for Food Safety Inspection Technology, Tianjin 300457, China*
[5]*Tianjin Key Laboratory of Epigenetics for Organ Department in Preterm Infants, The Fifth Central Hospital of Tianjin, Tianjin 300450, China*
[6]*College of Food Science and Engineering, Henan University of Technology, Zhengzhou 450001, China*
[7]*Department of Agriculture, Hetao College, Bayannur, Inner Mongolia, China*
[8]*College of Food Science and Technology, Hebei Normal University of Science and Technology, Qinhuangdao, Hebei 066004, China*

Correspondence should be addressed to Jing Li; ljcyhui@tust.edu.cn, Jilite Wang; 77560305@qq.com, Qingbin Guo; guoqingbin008322@tust.edu.cn, Suwen Liu; liusuwenyy@163.com, and Hao Wang; wanghao@tust.edu.cn

Received 28 July 2023; Revised 4 November 2023; Accepted 12 December 2023; Published 27 December 2023

Academic Editor: Kim Wei Chan

Ursolic acid (UA) is a natural triterpene carboxylic acid with an underlying anti-hyperlipidemia effect. This study examined the mechanism of interactions of UA with cholesterol esterase (CEase), pancreatic lipase (PL), and micellar cholesterol solubility *in vitro*. The half-maximal inhibitory concentration (IC_{50}) of CEase, PL, and micellar cholesterol solubility was determined to be 0.07 ± 0.01 mg/mL, 1.81 ± 0.13 mg/mL, and 1.73 ± 0.08 mg/mL, respectively. Multispectral combination revealed that UA changed the secondary structure and quenched the intrinsic fluorescence by static quenching of the two enzymes. The interactions were exothermic reaction as determined by enthalpy. Furthermore, molecular docking confirmed that UA was bound to amino acids of two enzymes at active site through hydrophobic interaction and van der Waals forces. Molecular dynamics (MD) simulation found that CEase and PL rearranged with UA to form stable complexes. The strong inhibition effect of CEase and PL mediated by UA might provide additional insight into understanding the role of UA in the hypolipidemic effect.

1. Introduction

Hyperlipidemia is a disease characterized by abnormal lipid metabolism, and excessive lipid accumulation predisposes to infection with atherosclerosis [1]. In the process of adipogenesis, cholesteryl esterase (CEase) and pancreatic lipase (PL) in the small intestine are the essential enzymes associated with hyperlipidemia, converting dietary fat into more readily absorbed free cholesterol, monoacylglycerol, and fatty acids [2, 3]. These molecules form mixed cholesterol micelles with bile salts, crossing the brush border membrane of the enterocyte and further entering the lymphatic system to participate in circulation [4, 5]. Inhibiting CEase and PL activity is expected to decrease

lipids levels and the risks of related diseases. Orlistat is widely used in clinical practice as a special kind of CEase and PL inhibitor. It effectively reduces the incidence of obesity-related diseases, whereas long-term use will induce a number of side effects including diarrhea, nausea, vomiting, and fatty stool [6–8]. Thus, exploring alternative plant-derived natural inhibitors may be an approach to prevent hyperlipidemia with bright prospects.

Plants have always been a treasure trove of bioactive compounds with diverse therapeutic relevance. Triterpenes, in the form of free glycosides or esters in plants, play a role in regulating blood lipid composition and reducing lipid accumulation. Studies have shown that some naturally derived triterpene saponins had promising inhibitory effects on intestinal esterase activity and lipid accumulation [9–11]. Ursolic acid (UA) is a natural triterpene carboxylic acid, widely found in the leaves and fruits of the *Rhododendron* family [12, 13]. It has a lot of pharmacological effects, including anti-hyperlipidemic, anti-atherosclerotic, and alleviating alcoholic liver injury [14, 15]. The antiobesity properties have also been documented by inhibiting adipogenesis in 3T3-L1 adipocytes and adipose tissue hypertrophy in high-fat diet-induced rats [16, 17]. The maslinic acid (MA), corosolic acid (CA), and oleanolic acid (OA), structurally similar isomers to UA, improved lipid-lowering biological activities through regulation of Sirt1/AMPK signaling pathway and the expression of *PPARγ*, *AdipoR1*, and *AdipoR2*, as well as inhibition of pancreatic lipase (PL) [18–21]. However, no reports have been available on the inhibition effect and mechanism of UA against CEase and PL.

Therefore, this study aimed to evaluate the inhibitory potential and binding affinity of UA on the two enzymes of CEase and PL. Inhibition kinetics and mixed micelle suppression were determined to discover the inhibition types and micelle conformation. Different techniques including isothermal titration calorimetry (ITC), florescent spectroscopy, Fourier-transform infrared spectroscopy (FTIR), and computer simulations were used to characterize the combined mechanism of UA with CEase and PL. The findings in this article will provide a relevant reference and theoretical basis to explore the functional food and application of UA to enhance the hypolipidemic effect.

2. Materials and Methods

2.1. Materials. Both cholesterol esterase (CEase) (300 unit/g solid) and pancreatic lipase (PL) (54 unit/mg solid) from porcine, *p*-nitrophenyl laurate (*p*-NPL), and orlistat were procured from Aladdin Chemical (Shanghai, China). Ursolic acid (≥95%) was purchased from Hunan Xianwei Industrial Co., LTD. (Changsha, China). *p*-Nitrophenyl butyrate (*p*-NPB) was purchased from Sigma-Aldrich Co. (St Louis, MO, USA). The cholesterol (CHO) kit was procured from Biosino Bio-technology and Science Inc. (Beijing, China). The other chemicals were of analytical grade.

2.2. CEase and PL Inhibitory Rates. The inhibitory rate of UA on CEase was calculated as described previously with slight modifications [22]. The configuration of *p*-NPB stock solution (20 mM) was carried out in acetonitrile. CEase was dissolved in 0.1 M PBS buffer (0.1 M NaCl, 5.16 mM sodium taurocholate, pH 7.0). Different concentrations of UA (0.01–0.15 mg/mL, 50 μL) were mixed with *p*-NPB (10 μL) and incubated at 310 K for 10 min. Then, CEase solution (0.54 mg/mL, 15 μL) was added to the system to initiate the enzyme reaction. After 5 min, the absorbance was measured with an ultraviolet spectrophotometer (UVmini-1240, Shimadzu Instrument Co., Japan) at 405 nm.

The inhibitory rate of UA against PL was analyzed as described earlier by Zhu et al. and Su et al. [23, 24]. A fixed concentration of the substrate *p*-NPL (0.8 mg/mL, 0.6 mL) and various amounts of UA (0.01–4 mg/mL) were mixed with Tris-HCl (0.1 M, pH 8.2). The mixed solution was incubated continuously at 310 K for 10 min. The reaction was initiated by adding PL initial solution (5 mg/mL, 200 μL). The absorbance value was detected (405 nm) after 20 min. Inhibitory rates were calculated according to the following equation:

$$\text{Inhibitory rate } (\%) = \left[1 - \left(\frac{C - D}{A - B}\right)\right] \times 100\%, \quad (1)$$

where A and B represent the absorbance values of control group and blank control group and C and D represent the absorbance values of experimental group and blank experimental group.

2.3. Inhibition Kinetics. The inhibition types of UA on cholesterol esterase and lipase were decided based on previous studies with minor modifications [25]. The reversible experiment of UA on CEase (0.5 mg/mL) and PL (5 mg/mL) was carried out at different UA concentrations (0, 0.03, 0.08, and 0.25 and 0, 0.7, 1.5, and 2.4 mg/mL, respectively). The velocity of the reaction versus the reciprocal of substrate concentration was recorded by the Lineweaver–Burk plot. UA with different concentrations was reacted with *p*-NPB (5, 10, 20, 40, 60, and 80 mM) and *p*-NPL (0.20, 0.30, 0.35, 0.40, 0.50, 0.80 mM) to analyze the inhibition mechanism of CEase and PL. The related parameters were calculated by following the Michaelis–Menten equation (equations (2) and (3)).

Competitive inhibition:

$$\frac{1}{V} = \frac{K_m}{V_m} \cdot \left(1 + \frac{[I]}{K_i}\right) \cdot \frac{1}{S} + \frac{1}{V_m}. \quad (2)$$

Mixed inhibition:

$$\frac{1}{V} = \frac{K_m}{V_m} \cdot \left(1 + \frac{[I]}{K_i}\right) \cdot \frac{1}{[S]} + \left(1 + \frac{[I]}{K_{is}}\right) \cdot \frac{1}{V_m}, \quad (3)$$

where V is the reaction velocity; V_m is the maximum reaction rate; $[S]$ is the *p*-NPB/*p*-NPL concentration; $[I]$ is the UA concentration; K_i is the inhibition constant of UA with CEase/PL; K_{is} is the inhibition constant of UA with enzyme-substrate complex; and K_m is the Michaelis–Menten constant.

2.4. Micellar Cholesterol Inhibition (MCI)

2.4.1. MCI Rate. The MCI was analyzed as described in method of Zhu et al. with slight modifications [26]. In brief, micelle solution contained PBS buffer (15 mM, pH 7.4), oleic acid (2.5 mM), taurocholate (10 mM), cholesterol (1 mM), and sodium chloride (132 mM). The solution was homogenized (400 W, 20 kHz, 30 min) by using ultrasonic homogenizer (UC-7100S, Meritech Technology (Tianjin) Co., LTD), and kept overnight at 310 K for later use. Then, the different UA concentrations (0, 0.25, 0.5, 1, 2, 3, and 4 mg/mL) or distilled water (control) was mixed with micellar solution at 310 K. After 2 h, sample solution was centrifuged at 8000g and collected in the supernatant. The cholesterol contents in micelles were measured by using a total cholesterol (TC) test kit. The MCI inhibition percent was calculated using the following equation:

$$\text{Inhibitory rate}\,(\%) = \frac{C_0 - C_1}{C_0} \times 100\%, \tag{4}$$

where C_0 is the cholesterol concentration in the absence of UA and C_1 is the cholesterol concentration in presence of UA.

2.4.2. Morphology. Dynamic light scattering (DLS) was used to analyze particle sizes of the mixed micelles by using a Zetasizer Nano ZS instrument (Brookhaven Instruments, Holtsville, UK). For each measurement, the micelles were not further treated by ultracentrifugation but diluted with distilled water at a rate of 1 : 2 (v/v, pH 7.4) [27]. Results were performed in triplicate as mean diameter (nm).

Transmission electron microscopy (TEM) was used to observe various atomic structures of solid materials by the fluctuation of electrons [27]. The micelles were diluted 50 times, and then 5 μL suspension was treated with a 200-mesh hole carbon support grid. Excess liquid was absorbed by the filter paper to form thin film, which was transferred into TEM (Talos G2 200X, Tokyo, Japan). The low electron beam was used as the light source and the electromagnetic field as the lens. Different light and dark images formed were displayed on vision systems after magnifying and focusing.

2.5. Fourier-Transform Infrared (FTIR) Spectra. The changes in secondary structure were studied by Thermo Nicolet IS50 FTIR Spectrometer (Thermo Nicolet Corp., USA). In brief, UA was incubated with CEase and PL separately at a rate 1 : 1 (v/v) for 15 min at 310 K and then lyophilized. After mixing with potassium bromide, samples were prepared by the pellet method. The wavelength range was 400 to 4000 cm^{-1} and resolution was 4 cm^{-1} [28]. Thermo Scientific OMNIC software was used for subtracting the blank background and smooth processing in the range of 1400–1800 cm^{-1} [7]. The second derivative fitting was performed using Origin. 9.0. The main peaks of the protein structure were further resolved by baseline automatic calibration and curve fitting [8].

2.6. Fluorescence Spectroscopy. The characteristic fluorescence of CEase and PL was detected using an F-7100 fluorescence spectrometer (HITACHI, Japan) based on a previous method [29]. The structures and quenching mechanisms between CEase (0.5 mg/mL) or PL (5 mg/mL) and UA were detected by analyzing the maximum fluorescence intensity change. The emission wavelength (λ_{em}) was 310 to 420 nm with fixed excitation wavelength (λ_{ex}) at 280 nm. The excitation and emission slits widths were all 5 nm. Fluorescence absorption peaks were recorded at different temperatures (298 K, 304 K, and 310 K), which were frequent and representative for analyzing the fluorescence quenching mechanism [7, 30].

The Stern–Volmer equation was used to analyze the fluorescence quenching ability [31]:

$$\begin{aligned}\frac{F_0}{F} &= 1 + K_q \tau_0 [Q] \\ &= 1 + K_{sv}[Q],\end{aligned} \tag{5}$$

where $[Q]$ represent the different concentrations of UA; τ_0 is the average lifetime of fluorescence without UA ($\tau_0 \approx 10^{-8}$ s); and K_{sv} and K_q represent the Stern–Volmer dynamic quenching constant and the quenching rate constant of UA on CEase and PL, respectively.

The Scatchard equation was used to analyze the binding strength [32]:

$$\lg\left[\frac{F_0 - F}{F}\right] = \lg K_a + n\lg[Q], \tag{6}$$

where F_0 and F represent the fluorescence intensity of the free CEase/PL and complex, respectively; n is the number of binding sites; and K_a is the binding constant.

2.7. Conformational Studies. To further investigate the quenching mechanism of characteristic amino acids more intuitively, synchronous and excitation-emission matrix (EEM) fluorescence method was followed [33]. Tyrosine (Tyr) and tryptophan (Trp) fluorescence intensities were recorded by varying difference excitation or emission wavelength range. The emission wavelengths (λ_{em}) of tryptophan and tyrosine were recorded in the continuous range of 265–420 nm and 220–420 nm, respectively, with fixed excitation wavelength (λ_{ex}) at 280 nm. The EEM spectra were collected with excitation and emission wavelength in the range of 200–500 nm.

2.8. Isothermal Titration Calorimetry (ITC). ITC was conducted using an ITC-200 calorimeter (Malvern, USA) as described by Wu et al. [34]. UA (135 μM) was set as the titrant, and CEase or PL solution (13.5 μM) was set as the sample solution. In all, 50 μL titrant was injected sequentially into the titration cell with CEase or PL solution (150 μL). The time interval of each injection was 150 s and lasted for 4 s between successive injections. Origin 9.0 was used for standardization, including estimating thermodynamic parameters, fitting binding isotherms, and iterative curve fitting. The *Gibbs* free energy was analyzed by the following equation:

$$\Delta G = \Delta H - T\Delta S, \tag{7}$$

where ΔH and ΔS are enthalpy and entropy change, respectively, and T is the Kelvin temperature.

2.9. Molecular Docking. Molecular docking of UA with CEase and PL was simulated by Discover Studio 3.5 (DS3.5 Accelrys, USA). The 3D structures of CEase and PL were procured from the Protein Data Bank (CEase ID: 1AQL, PL ID: 1GPL, https://www.rcsb.org/pdb). The molecule structures of UA (CAS: 77-52-1), orlistat (CAS: 96829-58-2), *p*-NPB (CAS: 2635-84-9), and *p*-NPL (CAS: 1956-11-2) were downloaded from Chemical Book (https://www.chemicalbook.com). Water molecules were removed from CEase and PL, and missing hydrogen atoms were added before the simulation. The interaction model with the highest LibDock score was deemed as the optimal configuration.

2.10. Dynamic Simulation. Molecular dynamics simulation was performed using GROMACS 2021 to analyze the dynamic trajectories and stability of complex molecules [35]. It was considered as an important tool to explore the patterns of binding and interaction. The structures of the receptor and ligand were derived from the molecular docking results. Complex structures were immersed in the center of a cubic box (TIP3P water molecules). The charge was neutralized by sodium chloride under the AMBER14SB force field (310 K). Simulation files were output in 30,000 ps.

2.11. Statistical Analysis. Data analysis and plotting were performed with the software of OMNIC and Origin. 9.0. SPSS 26 was applied at a significant level of $p < 0.05$. Each measurement was repeated three times.

3. Results and Discussion

3.1. Inhibitory Effect of UA on CEase and PL. Enzyme activity inhibition experiments were carried out *in vitro* using orlistat as the positive control. As shown in Figures 1(a) (D) and 1(b) (E), the IC_{50} value of UA and orlistat on CEase was 0.07 ± 0.01 mg/mL and 0.003 ± 0.010 mg/mL, respectively. Similarly, the IC_{50} value of UA and orlistat to PL was 1.81 ± 0.13 mg/mL and 0.05 ± 0.02 mg/mL, respectively. Although less compared to orlistat, the inhibition effect of UA on CEase was higher than that of ginkgolide B (IC_{50}: 0.34 ± 0.02 mg/mL) [36], as well as that of UA on PL was higher than that of betulin (IC_{50}: 3.19 ± 0.11 mg/mL) and ginsenoside Rd (IC_{50}: 4.06 ± 1.41 mg/mL) [21].

3.2. Inhibition Types. The inhibition types of enzymes generally fall into two categories (reversible and irreversible inhibition) [37]. The relationships between enzyme concentration and reaction rate with different UA concentrations are shown in Figures 1(a) (B) and 1(b) (B). All curves of V versus CEase and PL concentration passed through the origin as the concentration of UA increased, indicating that the inhibitions of UA against CEase and PL were reversible and the binding was noncovalent.

The Lineweaver–Burk plots were used to explore the inhibition mechanisms of UA on the two enzymes. With an increase in UA concentration, the four Lineweaver–Burk lines intersected in the second quadrant, the K_m value increased, and V_m gradually decreased (Figure 1(a) (C)). The inhibition type of UA on CEase was mixed inhibition, and UA was bound to the CEase-*p*-NPB to form the UA-CEase-*p*-NPB ternary compound. The inhibition constants K_i and K_{is} were 2.07 μM and 3.96 μM, respectively, in Figures 1(a) (D) and (E). The binding affinity of UA with free CEase was greater than that of the CEase-*p*-NPB complex ($K_i < K_{is}$). In case of PL, all the straight lines exhibited in Figure 1(b) (C) intersected on the Y-axis. The K_m values gradually increased with increased UA concentration (Table S1), suggesting that the inhibition type of UA on PL was competitive. UA might bind to the PL active site region by inducing the structural change and decreasing catalytic activity of PL [37].

3.3. MCI Analysis. Micelle formation is a pivotal step in the absorption of fatty acids and cholesterol in the small intestine [26]. The MCI was evaluated by preparing artificial micelles (Figure 2(a)). In the supernatant obtained by ultracentrifugation, significant dose-dependent inhibition of micellar solubility was determined with the addition of UA (IC_{50}: 1.73 ± 0.08 mg/mL). The size of micellar particles increased with the addition of UA as shown in Figure 2(b). The average particle size of micelles increased from 47 nm to 700 nm with the PDI value increasing. The larger the PDI, the wider the molecular weight distribution [38]. Results indicated that UA destroyed the micelle homogeneous state in the solution.

As shown in Figures 2(c) and 2(d), the former as control micelles showed orbicular droplets and the specimens in the presence of UA generated anomalous particles. The spheroidal structure of micelles was destroyed and cholesterol was released from mixed micelle after treating with UA, suggesting that UA had a considerably destructive potential toward micelle conformation and strong inhibition of cholesterol incorporation in soluble micelles. The most likely reason for the elimination of cholesterol from micelles was due to the hydrophobic interactions with bile salt [39].

3.4. FTIR Spectra. FTIR spectra were used to obtain information about the secondary structure of CEase and PL. As shown in Figure 3(a), the amide I band peak position of CEase was changed from 1654 to 1648 cm^{-1} with the addition of UA while the amide II band shifted from 1541 to 1552 cm^{-1}. The changes of peak positions illustrated the relocation of the hydrogen bonding pattern and the secondary conformation changes of CEase. In Figure 3(b), the amide I band peak of PL was changed from 1652 to 1648 cm^{-1} while the amide II band peak changed from 1546 to 1543 cm^{-1}. Both the amide I and II band peaks showed a blue shift, which revealed that UA decreased the polarity of PL in solution and enhanced the hydrophobicity.

Through curve fitting amide I band, the percentage of each secondary structure was estimated for further quantitative comparison. Free CEase constituted 34.49% α-helix,

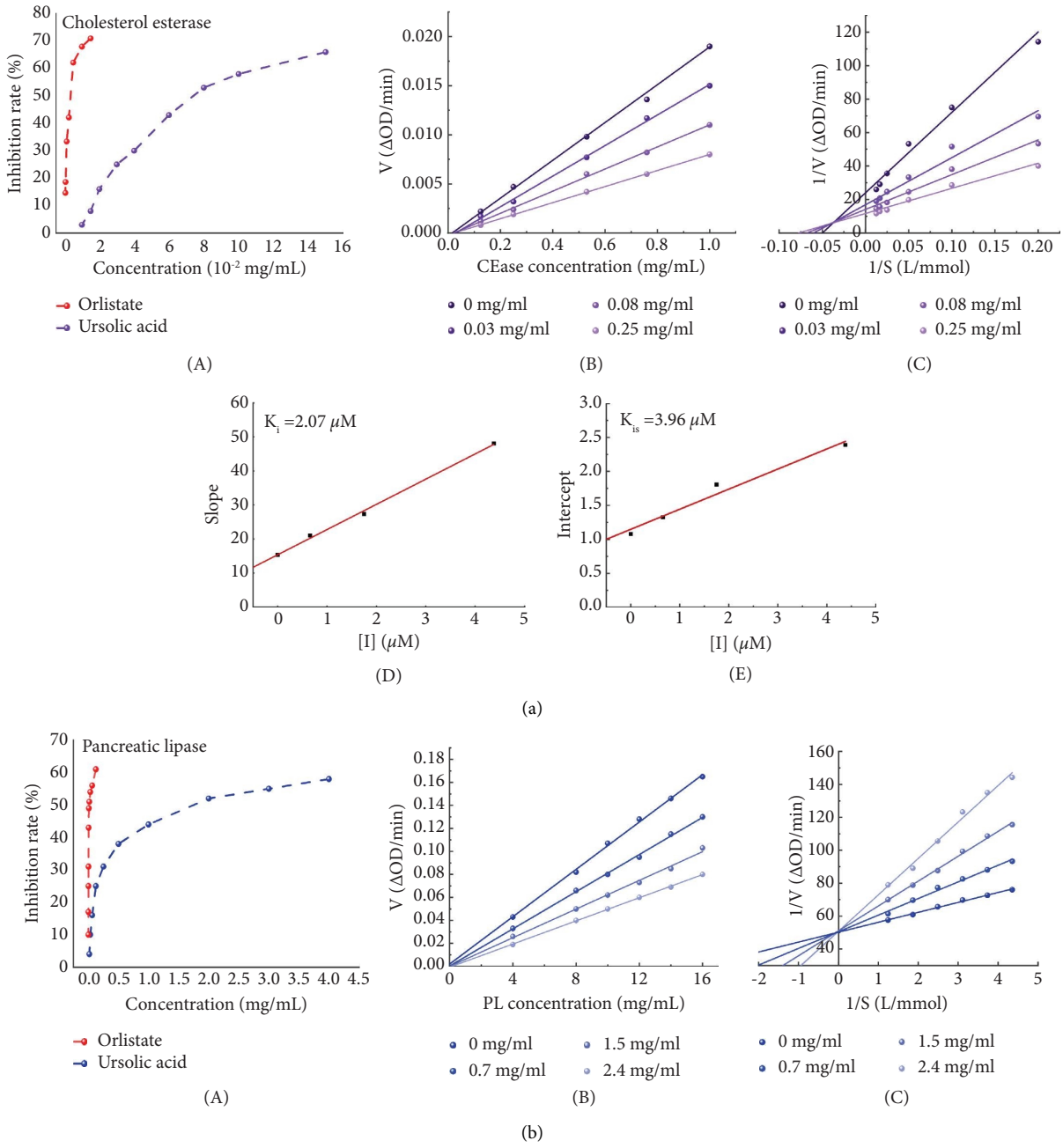

Figure 1: Inhibition types and kinetics of UA on CEase (a) and PL (b). The inhibition rate (A) of CEase and PL by UA and orlistat; reversible test plots (B) of CEase and PL; Lineweaver–Burk plots (C) of UA on CEase and PL. Inset: the linearly fitted secondary plots of slope (D) or intercept versus [*I*] (E) of CEase.

17.48% β-sheet, 27.66% β-turn, 12.54% β-antiparallel, and 7.83% random helix in Figure 3(a), showing that the α-helix was the most abundant structure of amino acids and acted as a scaffold to equilibrate the steric configuration of CEase [40]. In case of CEase-UA, the contents of β-sheet, α-helix, and β-antiparallel were decreased to 13.72%, 26.98%, and 10.44%, respectively. Meanwhile, the α-helix contents of PL-UA were reduced to 42.85% (Figure 3(b)). According to previous studies, the formation of the intermolecular hydrogen bond was related to the β-sheet structure [41]. The decreased β-sheet indicated a more flexible molecular structure. Alteration in FTIR spectra reflected that UA interfered with the hydrogen bonding networks of CEase and PL, and thus the secondary structure of the two enzymes was rearranged.

3.5. Fluorescence Quenching. Fluorescence spectroscopy is a sensitive instrument to evaluate the tertiary structure characteristics of CEase and PL. The fluorescence intensity was closely associated with phenylalanine, tryptophan, and tyrosine. The excitation and emission light of the

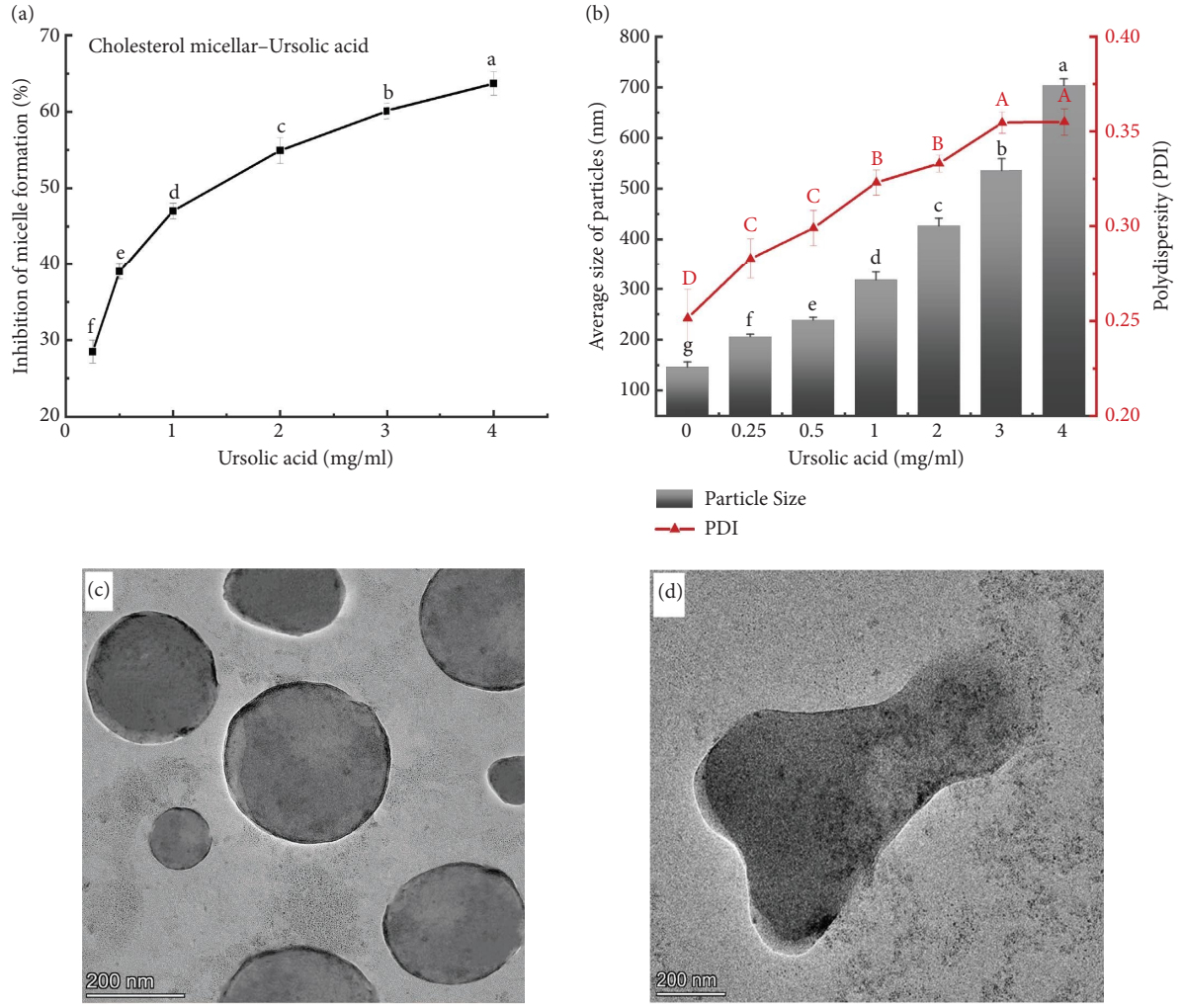

FIGURE 2: (a) The micelle solubility inhibition rate; (b) variation of micelle size and polydispersity index; (c) control micelles without UA; (d) micelles plus 0.5 mg/mL UA. Each measurement was repeated three times and data are presented as mean ± SD.

fluorophores (or both) might be affected by UA, so the values of all fluorescence intensity were corrected to avoid the inner filter effect [42]. Maximum fluorescence peaks were reduced with increased UA concentration (Figures 3(c) and 3(d)). This suggests that UA had a significant quenching effect on key lipid-digestive enzymes. The intrinsic fluorescence of CEase and PL was decreased by 58.18% and 14.29%, respectively, at 0.5 mg/mL UA, implying that the fluorescence quenching ability of UA on CEase was stronger than PL.

Stern–Volmer curves and Scatchard equation curves were curve-fitted to analyze the mechanism of fluorescence quenching. A good linear relationship of F_0/F versus [Q] indicated that the intrinsic fluorescence of CEase and PL quenched by UA existed in a single quenched manner (dynamic or static). In Table 1, the quenching constant K_q of CEase and PL was 1.892 ± 0.052 and 1.622 ± 0.294 ($\times 10^{11}$ L·mol^{-1}·s^{-1}), respectively. K_q was much larger than the maximum scatter collision quenching constant (2×10^{10} L·mol^{-1}·s^{-1}), forming slower diffusion and more ground-state complexes at high temperatures. The K_{sv} values of UA to CEase or PL decreased gradually with rising temperature, suggesting that a static quenching happened by forming an enzyme-UA complex.

The binding interaction parameters of UA and enzymes were investigated using the Scatchard equation. The results are shown in Table 1. The values of binding constant (K_a) of UA on CEase and PL were 1.892 ± 0.052 and 1.622 ± 0.294 ($\times 10^5$ L/mol) at 310 K, respectively. UA could bind well to CEase and PL to reduce the activity of both enzymes *in vivo* at the optimal temperature (310 K) [43, 44]. The values of K_a decreased with the elevated temperature to inhibit the production of complexes [45], which further explained the static quenching effect of UA on CEase and PL. In addition, the value of n approximately equal to one meant that UA had at least one high-affinity binding site in CEase or PL [46].

3.6. Conformational Analysis

3.6.1. Synchronous Fluorescence. Synchronous fluorescence quenching is commonly related to hydrophobic alteration regarding the major amino acid including tyrosine (Tyr) and

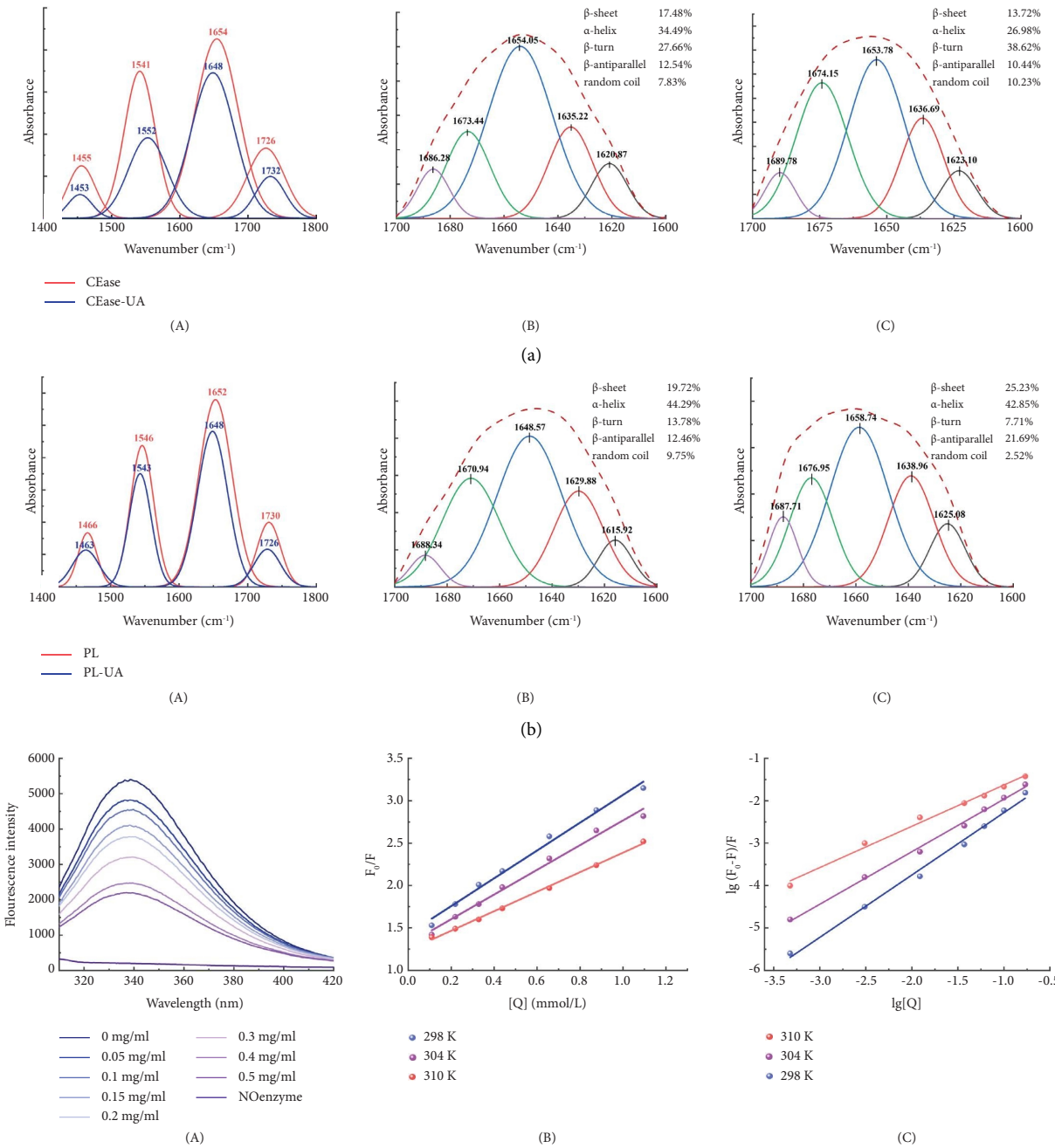

Figure 3: Continued.

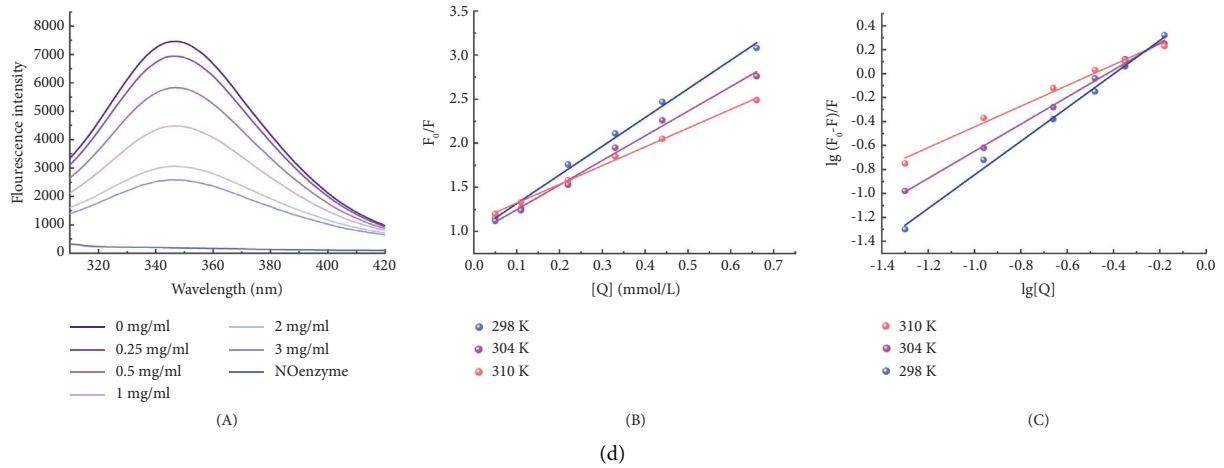

Figure 3: (a, b) Computer deconvolutions of the FTIR spectra in the region of 1800–1400 cm^{-1}. The amide *I* of free enzyme (B) and complex (C) ranged from 1700 to 1600 cm^{-1}. Fluorescence emission spectra of CEase (c) with different UA concentrations (0, 0.05, 0.10, 0.15, 0.20, 0.30, 0.40, and 0.50 mg/mL). Fluorescence emission spectra of PL (d) with different UA concentrations (0, 0.25, 0.50, 1.00, 2.00, and 3.00 mg/mL). Stern–Volmer plots (B) of UA against CEase and PL. The double logarithm regression curve (C) of L_g $[(F_0 - F)/F]$ versus L_g [Q] of CEase and PL.

Table 1: Fluorescence quenching parameters (K_{sv}, K_q, K_a, and n) of CEase-UA and PL-UA.

	T (K)	$K_{sv} \times 10^3$ (L/mol)	R^a	$K_q \times 10^{11}$ (L/mol·s)	$K_a \times 10^5$ (L/mol)	n	R^b
CEase	298	3.592 ± 0.157	0.990	3.592 ± 0.157	3.138 ± 0.127	0.938 ± 0.036	0.992
	304	3.190 ± 0.147	0.989	3.190 ± 0.147	2.157 ± 0.051	0.923 ± 0.033	0.996
	310	2.522 ± 0.041	0.997	2.522 ± 0.041	1.892 ± 0.052	0.928 ± 0.032	0.998
PL	298	2.255 ± 0.134	0.991	2.255 ± 0.134	2.614 ± 0.302	1.042 ± 0.046	0.994
	304	1.729 ± 0.118	0.991	1.729 ± 0.118	2.023 ± 0.282	0.931 ± 0.029	0.996
	310	0.562 ± 0.050	0.996	0.562 ± 0.050	1.622 ± 0.294	0.912 ± 0.044	0.986

[a]Correlation coefficient for the K_{sv} values. [b]Correlation coefficient for the K_a values.

tryptophan (Trp) residues [47]. Changes in the fluorescence intensity of Tyr ($\Delta\lambda = 15$ nm) and Trp ($\Delta\lambda = 60$ nm) in CEase in response to different UA concentrations are shown in Figures 4(a) and 4(b). The Trp fluorescence intensity was decreased more significantly than the Tyr at $\Delta\lambda = 15$ nm. The binding process mainly quenched the Trp residue fluorescence, and the binding site of UA was more pronounced close to Trp. Trp fluorescence peak underwent a blue shift from 283 to 278 nm, showing that UA might disturb the microenvironment to the active site, inducing the exposure of the hydrophobic surface.

Synchronous fluorescence spectra of the interaction between UA and PL are shown in Figures 4(c) and 4(d). UA strongly quenched the fluorescence intensity of both Trp and Tyr in PL. Trp fluorescence peak shows a red shift from 290 to 296 nm with increasing amounts of UA. The result suggests that UA reinforced the polarity of the microenvironment around Trp residues. Taken together, it was possible that UA interacted with the fluorophores of CEase and PL through hydrophobic interactions and hydrogen bonds, disturbed the microenvironment of amino acids at active sites, and further altered the tertiary structure of CEase and PL.

3.6.2. Excitation-Emission Matrix (EEM) Fluorescence Spectra. Fluorescence excitation-emission matrix spectra were used to reveal the comprehensive fluorescence structure of free CEase or PL and complexes. As shown in Figures 4(e)–4(h), peak 1 was the fluorescence intensity of the Trp and Tyr residues while peak 2 was the fluorescence intensity of the polypeptide-skeleton structure, respectively. Peaks a and *b* represented the first-order ($\lambda_{ex} = \lambda_{em}$) and second-order ($\lambda_{ex} = 2\lambda_{em}$) Rayleigh scattering, respectively [48].

As exhibited in Figures 4(e) and 4(f), peak 1 ($\lambda_{ex}/\lambda_{em}/I_n$, FI: 280/340/229 nm) and peak 2 ($\lambda_{ex}/\lambda_{em}/I_n$, FI: 225/340/261 nm) of CEase underwent fluorescence quenching, transforming to 280/340/120 and 230/335/87, respectively. Similarly, peak 1 ($\lambda_{ex}/\lambda_{em}/I_n$, FI: 280/345/1359 nm) and peak 2 ($\lambda_{ex}/\lambda_{em}/I_n$, FI: 230/340/2241 nm) of PL went down to 280/345/842 and 230/340/1069, respectively (Figures 4(g) and 4(h)). Compared with free enzymes, the decreased fluorescence intensity of peak 1 was observed with complex at various points of extent, which is in accordance to our results of steady-state fluorescence quenching. The decreased peak 2 showed that the UA caused the polypeptide backbone vibrates of enzymes by the $\pi \longrightarrow \pi^*$ transition [49]. Based on

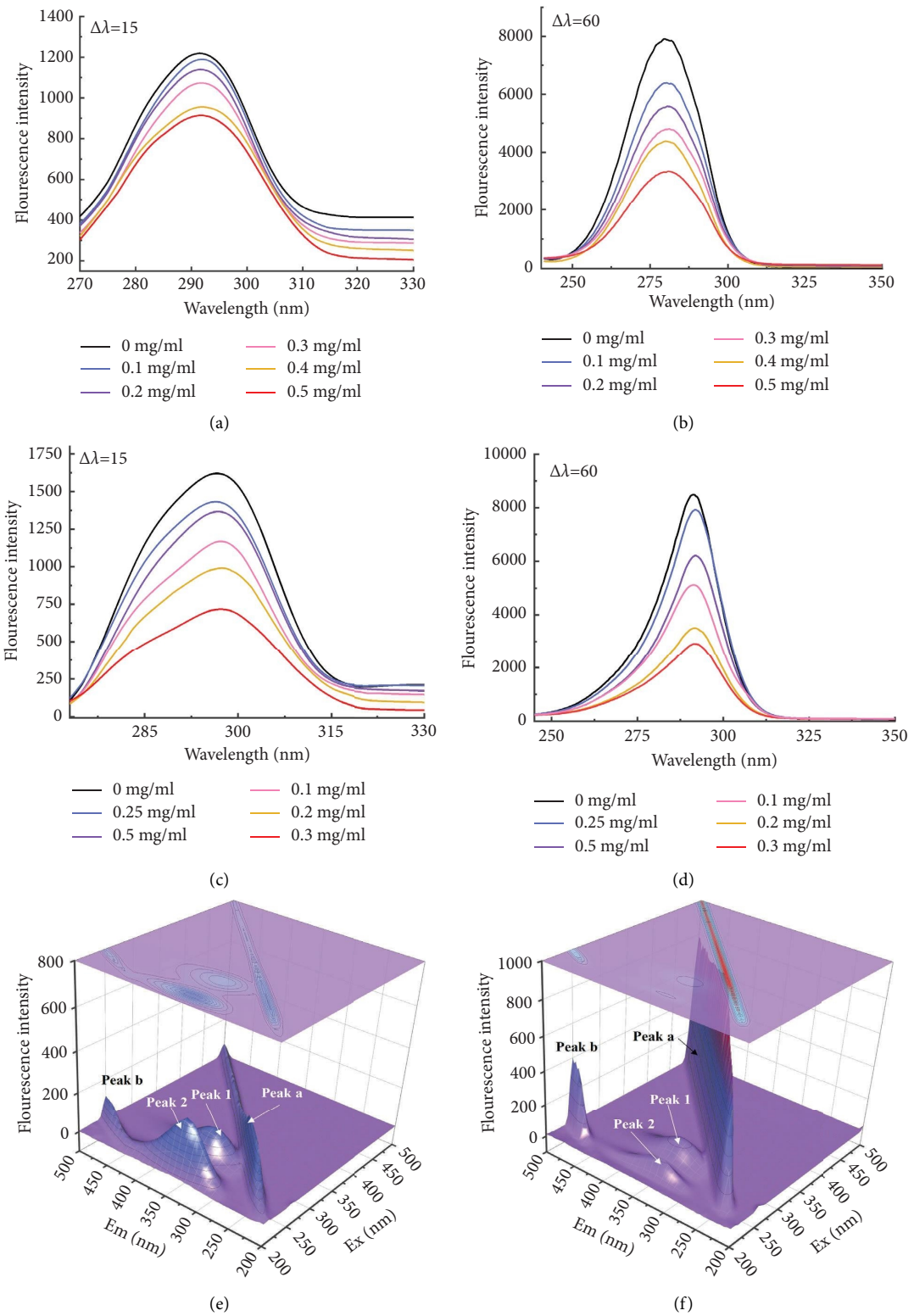

Figure 4: Continued.

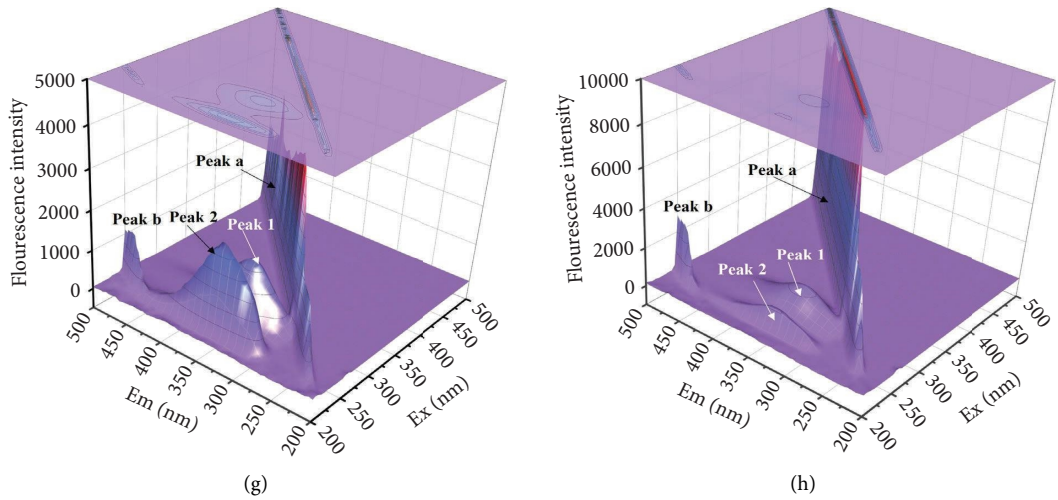

Figure 4: Synchronous and EEM fluorescence spectra of UA on CEase and PL. The variation of tyrosine (Tyr, $\Delta\lambda = 15$ nm) fluorescence intensity of CEase (a) and PL (c). The variation of tryptophan (Trp, $\Delta\lambda = 60$ nm) fluorescence intensity of CEase (b) and PL (d). The EEM fluorescence of free CEase (e), CEase-UA (f), PL (g), and PL-UA (h) along with the contour plots (on top).

the above results, the incorporation of UA quenched the intrinsic fluorescence of CEase and PL, thereby affecting the structure and activity of enzymes.

3.7. Isothermal Titration Calorimetry (ITC). ITC was used to monitor and record the calorimetric curves and thermodynamic parameters of protein-ligand interactions [50]. The curves of binding isotherms and corresponding heat flow versus time were obtained by injecting aliquots of UA solution into CEase (Figure 5(a)) and PL (Figure 5(b)). The decreased binding isotherms of UA on Cease/PL showed that the interaction was typically exothermic. The number of available binding sites on CEase/PL was relatively reduced. Negative ΔG of CEase (−7.67 kJ/mol) and PL (−6.33 kJ/mol) at applied temperatures indicated a spontaneous complexation process (Table S2). Also, the negative ΔH and ΔS demonstrated that hydrogen bond and van der Waals forces were dominant in the interaction of UA on CEase and PL. The value of ΔH was much lower than that of covalent bond energy (200–400 kJ/mol), further verifying that the interactions of UA with CEase or PL were noncovalent. The high affinity constants (K_{itc}) of CEase-UA and PL-UA, 4.09 and 3.15 ($\times 10^5$ L/mol), suggested a strong binding, and further studies were needed to analyze the type of actions. K_{itc} of PL-UA was slightly lower than that of CEase-UA and UA had a stronger affinity with CEase at 298 K in comparison with PL. K_{itc} was higher than binding constant (K_a) values shown in Table S2, which might be due to the diversity in sensitivity of experimental instruments [32].

3.8. Molecular Simulation

3.8.1. Molecular Docking and Binding Energy. To further confirm the above experimental findings at the molecular level, the conformation with the highest LibDock score was used to analyze the interaction of macromolecules with inhibitors [51]. The CEase-UA corresponding to the most stable conformations is supplemented in Figure 6(a). Ligands were located within the active pocket of CEase and surrounded by the hydrophobic residues (Leu, Trp, Phe, and Ala) in this region. The active site of PL contained the catalytic triad Ser152, Asp176, and His 263 [52]. The favorable binding conformation and binding site of the complex were directly observed in Figure 6(b). On locating the potential binding sites, UA formed pi-sigma and van der Waals force with His263 and Ser152, respectively. The results confirmed that CEase and PL were catalytically active only in specific steric conformations and UA binds to amino acids at the active sites of both enzymes to reduce the catalytic activity. The negative average value shown in Table 2 suggested that the binding was stable (CEase-UA, -32.26 ± 14.51 kJ/mol, and PL-UA, -24.69 ± 11.12 kJ/mol) [32]. The higher van der Waals energy and lower electrostatic energy suggested that the stability of CEase-UA and PL-UA mainly depended on van der Waals, which was consistent with the negative ΔH and ΔS in ITC analysis (Figure 5 and Table S2).

3.8.2. Molecular Dynamics Simulation. Molecular dynamics simulations were analyzed to investigate the molecular arrangement of the optimal docking conformation system. Previously, it was found that when the fluctuation of the root mean square deviation (RMSD) was relatively constant within 1 Å, a stable state of dynamic equilibrium could be achieved, and the lower RMSD value made the protein structure more stable [35]. With the extension of simulation time, the RMSD values of free CEase and CEase-UA were 2.21 and 2.15, respectively (Figure 7(a)). On the other hand, the value of PL-UA (1.86) was slightly higher than that of PL (1.84) in Figure 7(b). Results demonstrated that the difference between the two was negligible, which might be due to the disorderly movement of atoms caused by the surface temperature and the presence of water molecules in the molecular dynamics [53].

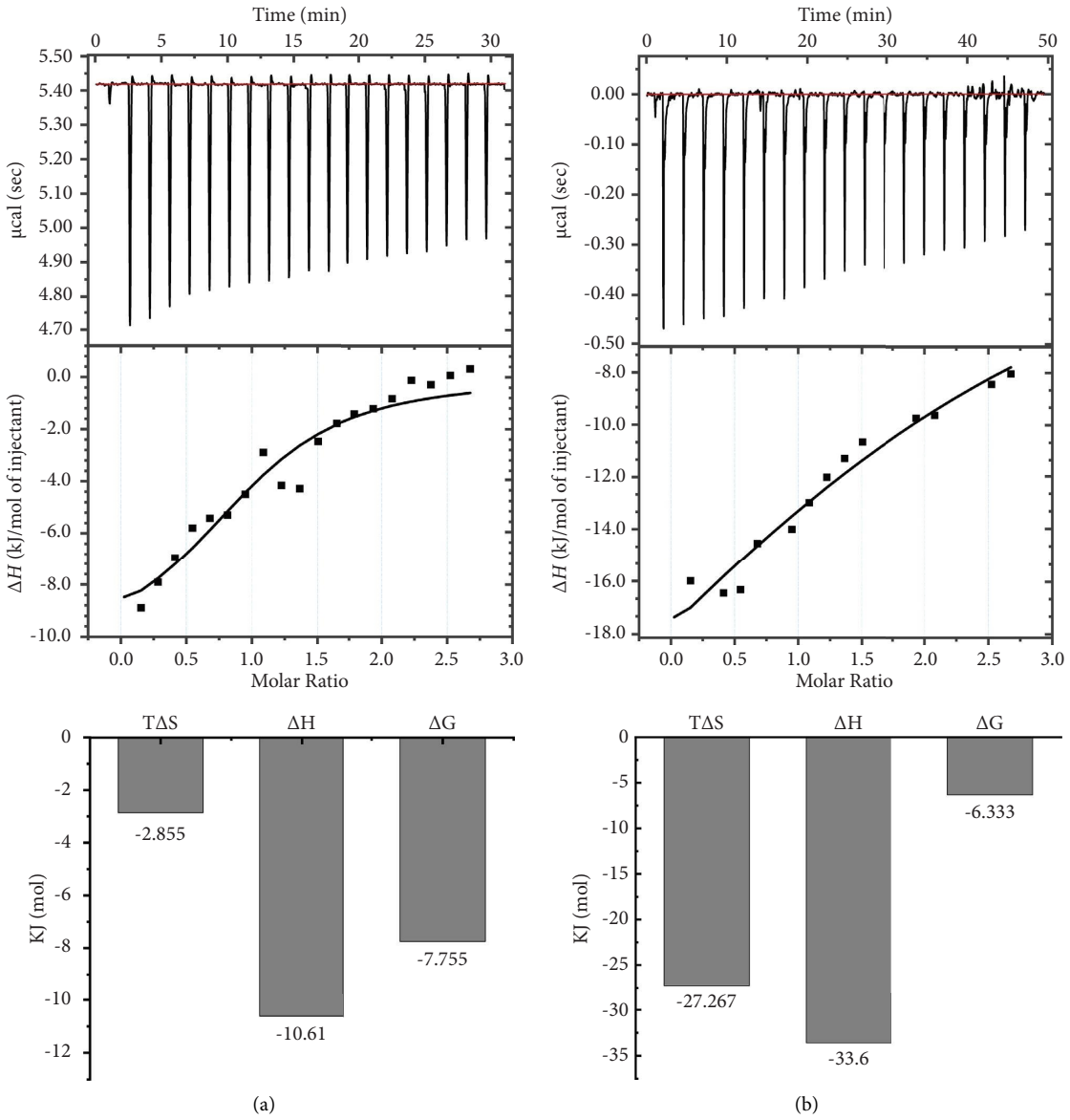

Figure 5: ITC for UA binding to CEase (a) and PL (b) at 298 K: (upper) raw data plot of titration heat flow with time (sec); (below) total heat released by titration with UA concentration. The black line indicates the least squares regression best-fit line. The histogram shows the changes in the thermodynamic parameters.

The root mean square fluctuation (RMSF) was used to characterize the structural flexibility of amino acids through fluctuations in residuals. The residues of CEase-UA and PL-UA fluctuated in the range of 0.5–3.0 Å (Figures 7(c) and 7(d)) which indicated that the results were rational. The changes in peak values indicated the flexibility and volatility of amino acid residues in aquatic environments (Figures 7(c) and 7(d)) [45]. The values of catalytic site amino acid for Phe324 (CEase) and His263 (PL) were 1.121 Å, 0.884 Å, 0.877 Å, and 0.504 Å for CEase, CEase-UA, PL, and PL-UA complex, respectively, which meant that the addition of UA enhanced the structure stability for both CEase and PL [54]. It suggested that the interaction had little effect on the stability of CEase while it stabilized the structure of PL.

The radius of gyration (Rg) was used to determine the tightness of the complexes of ligand and protein. As shown in Figure 7(e), the average values of Rg for the free enzyme (23.6) are higher than those of CEase-UA (23.4), indicating that the insertion of UA tightened the structure of CEase. The average Rg of the PL-UA system was decreased compared with that of free PL (Figure 7(f)). Mutual repulsion eventually leads to the extrusion of the double helix between the hydrophobic groups of PL and the hydrophilic residues of UA [32]. In general, the Rg values of the complex remained at a low level during the simulation. CEase and PL had good spatial compactness after combining with UA.

Solvent accessible surface area (SASA) is a parameter for estimating the exposure of amino acids to solvents, depending on the primary and secondary structure of the

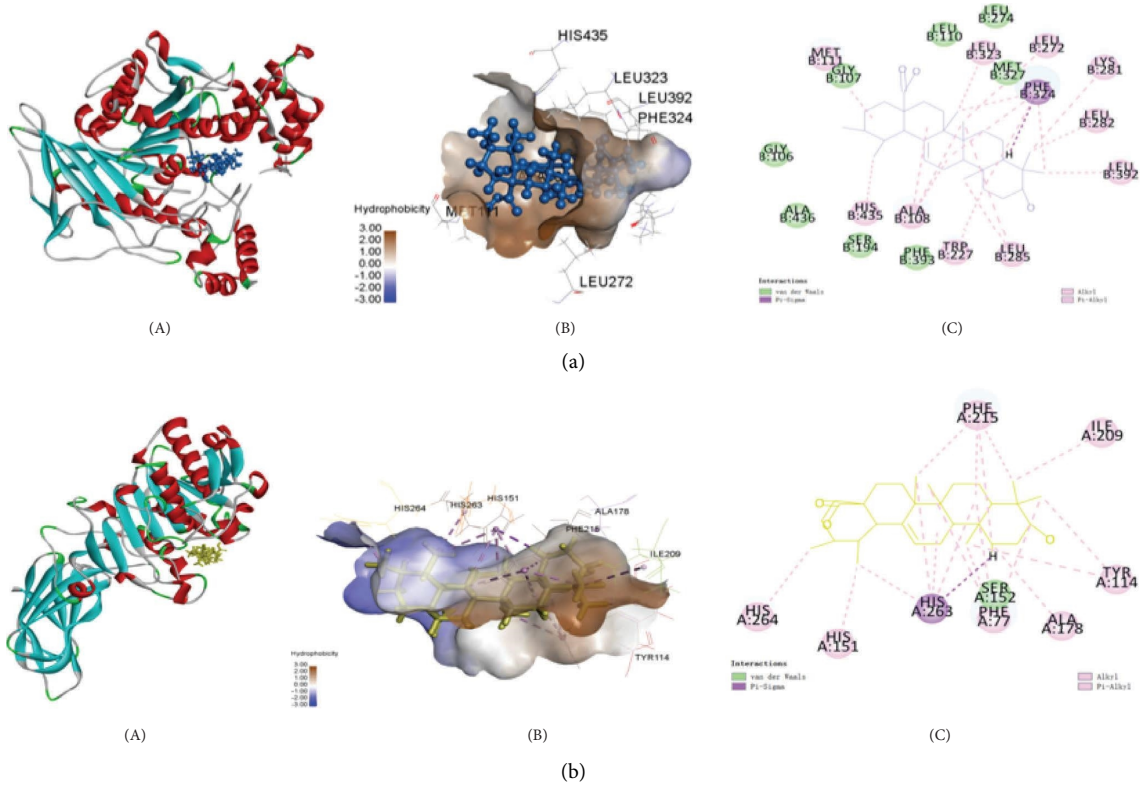

Figure 6: Molecular docking of CEase-UA (a) and PL-UA (b). The most appropriate confirmation (A), hydrophobic surface (B), and 2D schematic diagram (C). The interaction types are explained by the color of the legend.

Table 2: The averaged binding free energies of the simulated CEase-UA and PL-UA.

	Van der Waals (kJ/mol)	Electrostatic (kJ/mol)	Polar solvation (kJ/mol)	Nonpolar solvation (kJ/mol)	Binding energy (kJ/mol)
CEase-UA	−68.63 ± 7.34	−10.45 ± 8.61	70.53 ± 11.63	−23.71 ± 13.16	−32.26 ± 14.51
PL-UA	−54.52 ± 6.07	−12.86 ± 9.32	62.59 ± 10.21	−19.9 ± 14.48	−24.69 ± 11.12

Values were expressed as mean ± standard deviation.

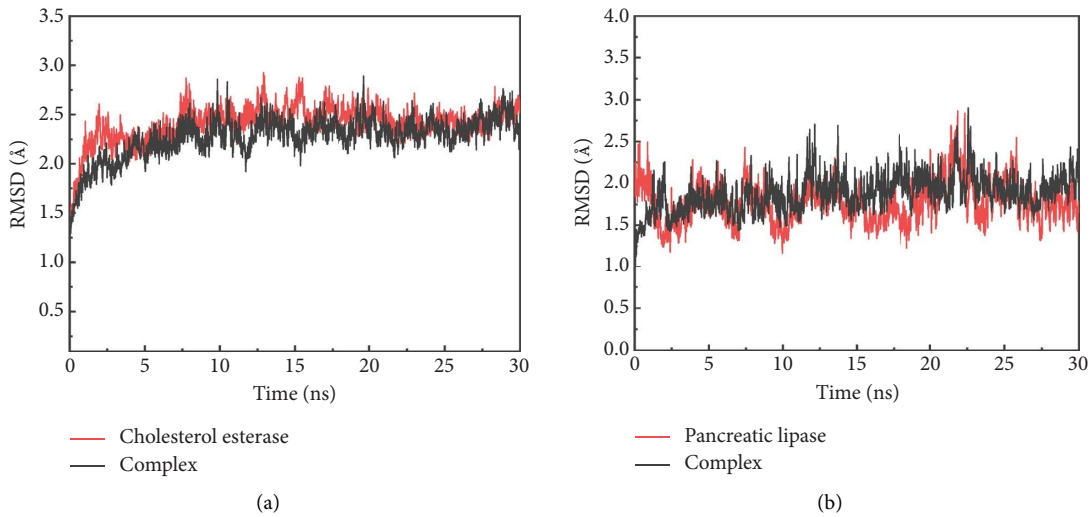

Figure 7: Continued.

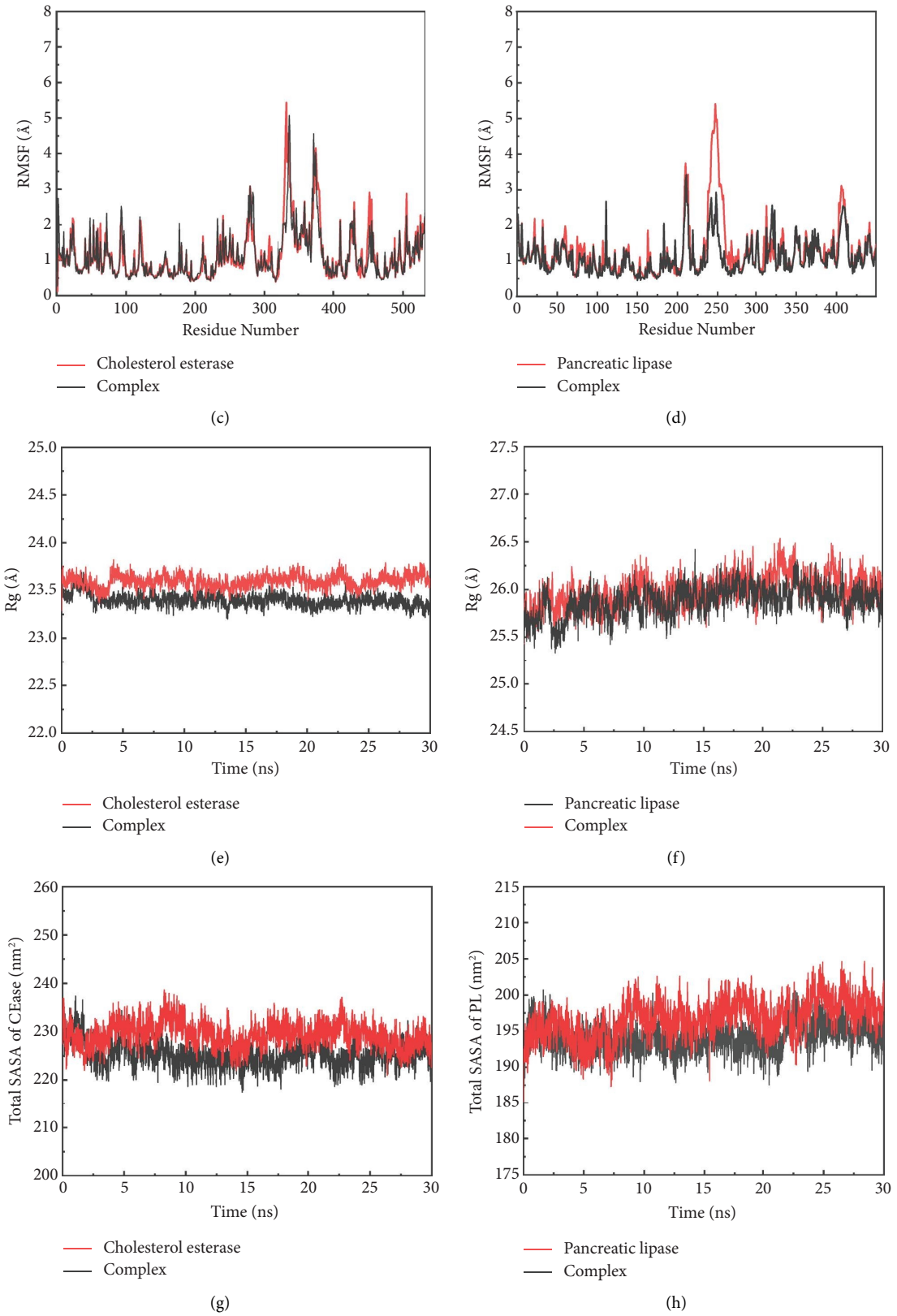

Figure 7: RMSD (a, b), RMSF (c, d), Rg (e, f), and SASA (g, h) of CEase and PL in free and combined states with UA.

protein [55]. Total SASA values of CEase-UA and PL-UA fluctuated less and the curve leveled off compared to those of the free enzymes in the 5–30 ns (Figures 7(g) and 7(h)), indicating that UA lowered the solvent accessible surface area of both enzymes to induce aggregation of the enzymes and molecular rearrangement. The MD simulation results showed that UA changed the structure of CEase and PL by reducing the flexibility of conformation, improving tightness and stability.

4. Conclusions

The study was aimed at exploring the inhibitory mechanism of UA on CEase, PL, and micellar cholesterol solubility. UA inhibited CEase and PL by mixed and competitive types, respectively, and decreased cholesterol micelle solubility by disrupting regular shape of mixed micelles. FTIR spectra and fluorescence spectra confirmed that UA perturbed the secondary and tertiary structure of enzymes and quenched tryptophan and tyrosine fluorescence by static quenching. Molecular simulations identified that UA bonded to amino acids at active site of the two enzymes to form good stability and tightness. This study provided a useful theoretical basis for the development and application of UA in lipid-lowering functional food ingredients.

Abbreviations

CEase: Cholesterol esterase
PL: Pancreatic lipase
UA: Ursolic acid
MCI: Micellar cholesterol inhibition
p-NPB: *p*-Nitrophenyl butyrate
p-NPL: *p*-Nitrophenyl laurate
IC_{50}: Half-inhibitory concentration
FTIR: Fourier-transform infrared spectroscopy
ITC: Isothermal titration calorimetry
PDI: Polydispersity index
TEM: Transmission electron microscopy.

Data Availability

The data used to support the findings of this study are included within the article.

Conflicts of Interest

The authors declare that there are no conflicts of interest.

Authors' Contributions

Wenjing Jiang and Hao Wang were responsible for conceptualization. Wenjing Jiang, Qun Huang, and Xiangxing Meng were responsible for methodology. Wenjing Jiang, Rizwan-ur Rehman, and Xu Yang were responsible for formal analysis. Wenjing Jiang, Kun Qian, Xiaozhi Liu, and Jingnan Chen were responsible for investigation. Wenjing Jiang, Rizwan-ur Rehman, and Ye Zhang were responsible for data curation and visualization. Wenjing Jiang was responsible for original draft preparation. Wenjing Jiang, Jilite Wang, Jing Li, and Hao Wang were responsible for review and editing. Rizwan-ur Rehman, Qingbin Guo, Suwen Liu, and Hao Wang were responsible for supervision.

Acknowledgments

This work was supported by the Key Laboratory Fund of Guizhou Medical University (GMU-2022-HJZ-06) and the Open Project Program of State Key Laboratory of Food Nutrition and Safety, Tianjin University of Science and Technology (SKLFNS-KF-202201).

Supplementary Materials

Table S1: V_m and K_m of UA inhibiting CEase and PL. Table S2: thermodynamics parameters of CEase-UA and PL-UA from ITC. (*Supplementary Materials*)

References

[1] C. Fu, Y. Jiang, J. Guo, and Z. Su, "Natural products with anti-obesity effects and different mechanisms of action," *Journal of Agricultural and Food Chemistry*, vol. 64, no. 51, pp. 9571–9585, 2016.

[2] M. Makran, N. Faubel, G. López-García et al., "Sterol bioaccessibility in a plant sterol-enriched beverage using the INFOGEST digestion method: influence of gastric lipase, bile salts and cholesterol esterase," *Food Chemistry*, vol. 382, Article ID 132305, 2022.

[3] Z. Sattar, H. Iranfar, A. Asoodeh, M. R. Saberi, M. Mazhari, and J. Chamani, "Interaction between holo transferrin and HSA–PPIX complex in the presence of lomefloxacin: an evaluation of PPIX aggregation in protein–protein interactions," *Spectrochimica Acta Part A: Molecular and Biomolecular Spectroscopy*, vol. 97, pp. 1089–1100, 2012.

[4] F. C. Petry and A. Z. Mercadante, "Addition of either gastric lipase or cholesterol esterase to improve both β-cryptoxanthin ester hydrolysis and micellarization during in vitro digestion of fruit pulps," *Food Research International*, vol. 137, Article ID 109691, 2020.

[5] A. Sharifi-Rad, J. Mehrzad, M. Darroudi, M. R. Saberi, and J. Chamani, "Oil-in-water nanoemulsions comprising Berberine in olive oil: biological activities, binding mechanisms to human serum albumin or holo-transferrin and QMMD simulations," *Journal of Biomolecular Structure and Dynamics*, vol. 39, no. 3, pp. 1029–1043, 2021.

[6] S. Li, J. Pan, X. Hu, Y. Zhang, D. Gong, and G. Zhang, "Kaempferol inhibits the activity of pancreatic lipase and its synergistic effect with orlistat," *Journal of Functional Foods*, vol. 72, Article ID 104041, 2020.

[7] F. Kalhori, H. Yazdyani, F. Khademorezaeian et al., "Enzyme activity inhibition properties of new cellulose nanocrystals from *Citrus medica* L. pericarp: a perspective of cholesterol lowering," *Luminescence*, vol. 37, no. 11, pp. 1836–1845, 2022.

[8] R. Assaran Darban, B. Shareghi, A. Asoodeh, and J. Chamani, "Multi-spectroscopic and molecular modeling studies of interaction between two different angiotensin I converting enzyme inhibitory peptides from gluten hydrolysate and human serum albumin," *Journal of Biomolecular Structure and Dynamics*, vol. 35, no. 16, pp. 3648–3662, 2017.

[9] R. A. Mosa, J. J. Naidoo, F. S. Nkomo, S. E. Mazibuko, C. J. Muller, and A. R. Opoku, "In vitro antihyperlipidemic

potential of triterpenes from stem bark of Protorhus longifolia," *Planta Medica*, vol. 80, no. 18, pp. 1685–1691, 2014.

[10] J. Chamani, "Energetic domains analysis of bovine α-lactalbumin upon interaction with copper and dodecyl trimethylammonium bromide," *Journal of Molecular Structure*, vol. 979, no. 1-3, pp. 227–234, 2010.

[11] S. Hamed-Akbari Tousi, M. Reza Saberi, and J. Chamani, "Comparing the interaction of cyclophosphamide monohydrate to human serum albumin as opposed to holotransferrin by spectroscopic and molecular modeling methods: evidence for allocating the binding site," *Protein and Peptide Letters*, vol. 17, no. 12, pp. 1524–1535, 2010.

[12] L. Wang, Q. Yin, C. Liu, Y. Tang, C. Sun, and J. Zhuang, "Nanoformulations of ursolic acid: a modern natural anticancer molecule," *Frontiers in Pharmacology*, vol. 12, Article ID 706121, 2021.

[13] R. Taheri, N. Hamzkanlu, Y. Rezvani et al., "Exploring the HSA/DNA/lung cancer cells binding behavior of p-Synephrine, a naturally occurring phenyl ethanol amine with anti-adipogenic activity: multi spectroscopic, molecular dynamic and cellular approaches," *Journal of Molecular Liquids*, vol. 368, Article ID 120826, 2022.

[14] D. Kashyap, H. S. Tuli, and A. K. Sharma, "Ursolic acid (UA): a metabolite with promising therapeutic potential," *Life Sciences*, vol. 146, pp. 201–213, 2016.

[15] Ł. Woźniak, S. Skąpska, and K. Marszałek, "Ursolic acid—a pentacyclic triterpenoid with a wide spectrum of pharmacological activities," *Molecules*, vol. 20, no. 11, pp. 20614–20641, 2015.

[16] Y. He, Y. Li, T. Zhao, Y. Wang, and C. Sun, "Ursolic acid inhibits adipogenesis in 3T3-L1 adipocytes through LKB1/AMPK pathway," *PLoS One*, vol. 8, no. 7, Article ID 70135, 2013.

[17] M. R. Housaindokht, J. Chamani, A. A. Saboury, A. A. Moosavi-Movahedi, and M. Bahrololoom, "Three binding sets analysis of alpha-Lactalbumin by interaction of tetradecyl trimethyl ammonium bromide," *Bulletin of the Korean Chemical Society*, vol. 22, no. 2, pp. 145–148, 2001.

[18] C. J. Liou, Y. W. Dai, C. L. Wang, L. W. Fang, and W. C. Huang, "Maslinic acid protects against obesity-induced nonalcoholic fatty liver disease in mice through regulation of the Sirt1/AMPK signaling pathway," *The Federation of American Societies for Experimental Biology Journal*, vol. 33, no. 11, pp. 11791–11803, 2019.

[19] H. Luo, J. Shen, C. Chen et al., "Lipid-lowering effects of oleanolic acid in hyperlipidemic patients," *Chinese Journal of Natural Medicines*, vol. 16, no. 5, pp. 339–346, 2018.

[20] C. Xue, Y. Li, H. Lv et al., "Oleanolic acid targets the gut–liver axis to alleviate metabolic disorders and hepatic steatosis," *Journal of Agricultural and Food Chemistry*, vol. 69, no. 28, pp. 7884–7897, 2021.

[21] H. Yu, S. Dong, L. Wang, and Y. Liu, "The effect of triterpenoid saponins on pancreatic lipase in vitro: activity, conformation, kinetics, thermodynamics and morphology," *Biochemical Engineering Journal*, vol. 125, pp. 1–9, 2017.

[22] S. Zhao, Y. Wu, and L. Hu, "Identification and synthesis of selective cholesterol esterase inhibitor using dynamic combinatorial chemistry," *Bioorganic Chemistry*, vol. 119, Article ID 105520, 2022.

[23] W. Zhu, Y. Jia, J. Peng, and C. M. Li, "Inhibitory effect of persimmon tannin on pancreatic lipase and the underlying mechanism in vitro," *Journal of Agricultural and Food Chemistry*, vol. 66, no. 24, pp. 6013–6021, 2018.

[24] H. Su, Y. T. Ruan, Y. Li, J. G. Chen, Z. P. Yin, and Q. F. Zhang, "In vitro and in vivo inhibitory activity of taxifolin on three digestive enzymes," *International Journal of Biological Macromolecules*, vol. 150, pp. 31–37, 2020.

[25] H. Wang, J. Wang, Y. Liu, Y. Ji, Y. Guo, and J. Zhao, "Interaction mechanism of carnosic acid against glycosidase (α-amylase and α-glucosidase)," *International Journal of Biological Macromolecules*, vol. 138, pp. 846–853, 2019.

[26] W. W. Zhu and C. H. Tang, "Mild preheating improves cholesterol-lowering benefits of soy protein via enhancing hydrophobicity of its gastrointestinal digests: an in vitro study," *Food Hydrocolloids*, vol. 124, Article ID 107282, 2022.

[27] J. Su, H. Wang, C. Ma et al., "Hypolipidemic mechanism of gypenosides via inhibition of pancreatic lipase and reduction in cholesterol micellar solubility," *European Food Research and Technology*, vol. 242, no. 3, pp. 305–312, 2016.

[28] G. Zhang, Y. Ma, L. Wang, Y. Zhang, and J. Zhou, "Multispectroscopic studies on the interaction of maltol, a food additive, with bovine serum albumin," *Food Chemistry*, vol. 133, no. 2, pp. 264–270, 2012.

[29] J. Wang, J. Zhao, Y. Yan, D. Liu, C. Wang, and H. Wang, "Inhibition of glycosidase by ursolic acid: in vitro, in vivo and in silico study," *Journal of the Science of Food and Agriculture*, vol. 100, no. 3, pp. 986–994, 2020.

[30] Z. Malek-Esfandiari, A. Rezvani-Noghani, T. Sohrabi, P. Mokaberi, Z. Amiri-Tehranizadeh, and J. Chamani, "Molecular dynamics and multi-spectroscopic of the interaction behavior between bladder cancer cells and calf thymus DNA with rebeccamycin: apoptosis through the down regulation of PI3K/AKT signaling pathway," *Journal of Fluorescence*, vol. 33, no. 4, pp. 1537–1557, 2023.

[31] L. Li, H. Xu, J. Zhou, J. Yu, L. Copeland, and S. Wang, "Mechanisms underlying the effect of tea extracts on in vitro digestion of wheat starch," *Journal of Agricultural and Food Chemistry*, vol. 69, no. 29, pp. 8227–8235, 2021.

[32] X. Zhang, R. U. Rehman, S. Wang et al., "Blue honeysuckle extracts retarded starch digestion by inhibiting glycosidases and changing the starch structure," *Food and Function*, vol. 13, no. 11, pp. 6072–6088, 2022.

[33] W. Yang, F. Liu, C. Xu, F. Yuan, and Y. Gao, "Molecular interaction between (−)-epigallocatechin-3-gallate and bovine lactoferrin using multi-spectroscopic method and isothermal titration calorimetry," *Food Research International*, vol. 64, pp. 141–149, 2014.

[34] X. Wu, W. He, L. Yao et al., "Characterization of binding interactions of (−)-epigallocatechin-3-gallate from green tea and lipase," *Journal of Agricultural and Food Chemistry*, vol. 61, no. 37, pp. 8829–8835, 2013.

[35] W. Wang, N. Gan, Q. Sun et al., "Study on the interaction of ertugliflozin with human serum albumin in vitro by multispectroscopic methods, molecular docking, and molecular dynamics simulation," *Spectrochimica Acta Part A: Molecular and Biomolecular Spectroscopy*, vol. 219, pp. 83–90, 2019.

[36] S. A. Al-Zakaria, I. A. Thanon, and L. M. Saadallah, "Effect of Ginkgo biloba on lipid profile in hypertensive patients on Valsartan monotherapy," *Annals of the College of Medicine Mosul*, vol. 40, no. 2, pp. 29–33, 2018.

[37] X. Du, M. Bai, Y. Huang et al., "Inhibitory effect of astaxanthin on pancreatic lipase with inhibition kinetics integrating molecular docking simulation," *Journal of Functional Foods*, vol. 48, pp. 551–557, 2018.

[38] X. Zhang, Y. Lu, R. Zhao, C. Wang, C. Wang, and T. Zhang, "Study on simultaneous binding of resveratrol and curcumin to β-lactoglobulin: multi-spectroscopic, molecular docking

and molecular dynamics simulation approaches," *Food Hydrocolloids*, vol. 124, Article ID 107331, 2022.

[39] J. Su, H. Wang, C. Ma et al., "Hypocholesterolaemic mechanism of bitter melon aqueous extracts via inhibition of pancreatic cholesterol esterase and reduction of cholesterol micellar solubility," *International Journal of Food Sciences and Nutrition*, vol. 67, no. 1, pp. 20–28, 2016.

[40] Y. Lv, Q. Liang, Y. Li, X. Liu, D. Zhang, and X. Li, "Study of the binding mechanism between hydroxytyrosol and bovine serum albumin using multispectral and molecular docking," *Food Hydrocolloids*, vol. 122, Article ID 107072, 2022.

[41] H. Tang, P. Song, J. Li, and D. Zhao, "Effect of Salvia miltiorrhiza on acetylcholinesterase: enzyme kinetics and interaction mechanism merging with molecular docking analysis," *International Journal of Biological Macromolecules*, vol. 135, pp. 303–313, 2019.

[42] L. Sun, M. J. Gidley, and F. J. Warren, "The mechanism of interactions between tea polyphenols and porcine pancreatic alpha-amylase: analysis by inhibition kinetics, fluorescence quenching, differential scanning calorimetry and isothermal titration calorimetry," *Molecular Nutrition and Food Research*, vol. 61, no. 10, Article ID 1700324, 2017.

[43] J. Chamani, A. A. Moosavi-Movahedi, and G. H. Hakimelahi, "Structural changes in β-lactoglobulin by conjugation with three different kinds of carboxymethyl cyclodextrins," *Thermochimica Acta*, vol. 432, no. 1, pp. 106–111, 2005.

[44] M. Hosseinzadeh, S. Nikjoo, N. Zare, D. Delavar, S. Beigoli, and J. Chamani, "Characterization of the structural changes of human serum albumin upon interaction with single-walled and multi-walled carbon nanotubes: spectroscopic and molecular modeling approaches," *Research on Chemical Intermediates*, vol. 45, no. 2, pp. 401–423, 2019.

[45] P. Thayumanavan, S. Nallaiyan, C. Loganathan, P. Sakayanathan, S. Kandasamy, and M. A. Isa, "Inhibition of glutathione and s-allyl glutathione on pancreatic lipase: analysis through in vitro kinetics, fluorescence spectroscopy and in silico docking," *International Journal of Biological Macromolecules*, vol. 160, pp. 623–631, 2020.

[46] R. Zhang, Y. Liu, X. Huang, M. Xu, R. Liu, and W. Zong, "Interaction of a digestive protease, Candida rugosa lipase, with three surfactants investigated by spectroscopy, molecular docking and enzyme activity assay," *Science of the Total Environment*, vol. 622-623, pp. 306–315, 2018.

[47] Y. J. Ma, J. H. Wu, X. Li et al., "Effect of alkyl distribution in pyrazine on pyrazine flavor release in bovine serum albumin solution," *Royal Society of Chemistry Advances*, vol. 9, no. 63, pp. 36951–36959, 2019.

[48] P. Zhang, Z. Li, X. Wang et al., "Study of the enantioselective interaction of diclofop and human serum albumin by spectroscopic and molecular modeling approaches in vitro," *Chirality*, vol. 25, no. 11, pp. 719–725, 2013.

[49] Y. Ji, D. Liu, Y. Jin et al., "In vitro and in vivo inhibitory effect of anthocyanin-rich bilberry extract on α-glucosidase and α-amylase," *Lebensmittel-Wissenschaft and Technologie*, vol. 145, Article ID 111484, 2021.

[50] X. Li, H. Jiang, Y. Pu, J. Cao, and W. Jiang, "Inhibitory effect of condensed tannins from banana pulp on cholesterol esterase and mechanisms of interaction," *Journal of Agricultural and Food Chemistry*, vol. 67, no. 51, pp. 14066–14073, 2019.

[51] T. Dai, J. Chen, Q. Li et al., "Investigation the interaction between procyanidin dimer and α-amylase: spectroscopic analyses and molecular docking simulation," *International Journal of Biological Macromolecules*, vol. 113, pp. 427–433, 2018.

[52] J. Hermoso, D. Pignol, B. Kerfelec, I. Crenon, C. Chapus, and J. C. Fontecilla-Camps, "Lipase activation by nonionic detergents: the crystal structure of the porcine lipase-colipase-tetraethylene glycol monooctyl ether complex," *Journal of Biological Chemistry*, vol. 271, no. 30, pp. 18007–18016, 1996.

[53] Y. Lu, R. Zhao, C. Wang, X. Zhang, and C. Wang, "Deciphering the non-covalent binding patterns of three whey proteins with rosmarinic acid by multi-spectroscopic, molecular docking and molecular dynamics simulation approaches," *Food Hydrocolloids*, vol. 132, Article ID 107895, 2022.

[54] Z. Yu, R. Kan, H. Ji et al., "Identification of tuna protein-derived peptides as potent SARS-CoV-2 inhibitors via molecular docking and molecular dynamic simulation," *Food Chemistry*, vol. 342, Article ID 128366, 2021.

[55] J. Zhu, C. Wang, J. Gao, H. Wu, and Q. Sun, "Aggregation of fucoxanthin and its effects on binding and delivery properties of whey proteins," *Journal of Agricultural and Food Chemistry*, vol. 67, no. 37, pp. 10412–10422, 2019.